A Novel Thermal Mapping Technique using Nano-confinement Assisted Quantum Dots for Transient Cooling Applications

Khan Md. Rabbi, Christopher Borden, Shawn A. Putnam
Department of Mechanical and Aerospace Engineering
University of Central Florida, Orlando, FL 32816
khan.rabbi@knights.ucf.edu, borden@knights.ucf.edu, shawn.putnam@ucf.edu

ABSTRACT

During air or liquid cooling, thermal resistance of the devices is measured precisely from the thermal information at the junction. But existing thermal measurement technologies fall short because of highly transient events such as unstable vortex formation (air cooling) and bubble growth (two-phase liquid cooling). In solving this problem, this paper reports a novel and low-cost thermal mapping technique that can capture highly spatio-temporal temperature evolution at the solid-liquid interface. Essentially, a robust interface is fabricated with $CuInS_2$/ZnS Quantum dots (λ_{peak} = 550 nm and 750 nm) trapped inside nanopores (20 nm-30 nm) of a ceramic membrane (50 μm) and/or everyday use paper. It is observed that such nanoconfinement assisted Quantum dots provided sustained thermal photoluminescence coefficient (-0.1 nm/°C) at high number of heating-cooling cycle. This unique yet low cost thermal mapping technique is applied to capture thermal evolution during micro-droplet impingement cooling and hemiwicking flows through anisotropic wicks which showcase commendable spatio-temporal benefits.

KEY WORDS: Thermal mapping technique, Electronics cooling, Quantum dot, Droplet impingement, Hemiwicking

NOMENCLATURE

A	amplitude, mm
d	diameter, nm
E	energy, eV
f	frequency, Hz
I	Intensity, A.U.
k	Thermal conductivity, W/m-K
P	Power, W
t	time, ms
T	Temperature, °C

Greek symbols

λ	wavelength, nm
Δ	difference

Subscripts

x	longitudinal
y	transverse
s	surface
g	band gap

INTRODUCTION

With the ever-growing demand for more powerful, faster, and smaller electronic processing comes the need for increased cooling efficiency and new, creative exploitation of natural phenomena to extract as much heat wicking possible. In order to implement these new pioneering methods of nanoscale thermal cooling, technologies must be developed to quickly and efficaciously investigate, study, and document under a wide variety of applications.

For example, in two-phase liquid cooling, bubble dynamics, rewetting events can be really transient phenomena [1], [2]. To generate understanding of thermal evolution during these unsteady and random events, highly spatio-temporal imaging technologies must be deployed which are highly expensive, complex to calibrate. Some methods have already been developed showing the capacity to conduct ultrafast imaging [3] utilizing quantum dot processing. Refining these technologies into a reusable and low-cost process would be an invaluable asset to interfacial research. Equipment has been developed utilizing quantum dot technology by employing Cadmium-Telluride (CdTe) and Cadmium-Selenide (CdSe) based structures because of their great temperature sensitivity and considerably better luminescence [4]–[7]. Other more specific photodetectors have been designed to detect mid-range light emissions, called mid-wavelength infrared detectors (MWIR), utilizing compounds such as Indium antimonide (InSb) and Mercury Cadmium Telluride (HgCdTe) [8] for their proven track record in other imaging technologies. Others use quantum dot technology to measure temperature changes in individual cells of tissue [9]. Very promising technologies have arisen as a result of quantum dot methodology, and extended research promises the possibility of ultrafast, sensitive and low-cost quantum dot alternatives to image processing [10]; creating a standard method of operation to construct a high resolution thermal diagnostic technique.

This paper reports such an inexpensive but effective technique to perform thermal mapping accurately at the solid-fluid interface. The photoluminiscence of differently sized quantum dots are utilized to get accurate thermal information. To achieve uniform coating, QDs are trapped into nanomembranes or everyday use paper by in-house dip-coating or drop-casting technique. With proper calibrations, the technique is then applied to micro-droplet impingement cooling and hemiwicking flows to showcase spatio-temporal benefits in temperature measurements.

METHODOLOGY

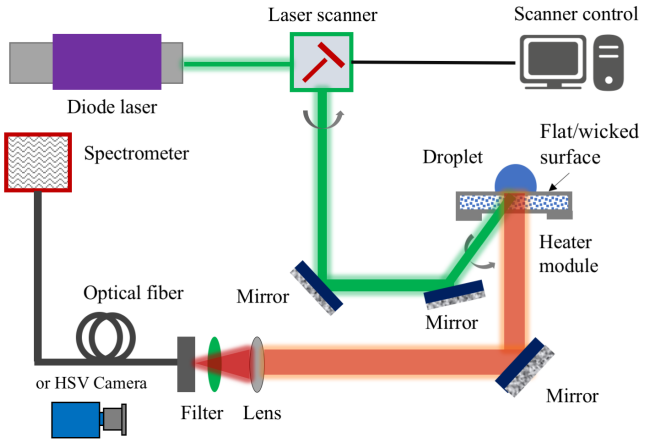

Fig. 1: Experimental scheme: High speed LASER scanner with an amplitudes of A_x, A_y = 100 mm, 80 mm and frequencies of f_x = 133 Hz, f_y = 533 Hz is employed to scan whole Region of Interest (ROI) to capture fluorescence from uniformly heated Quantum Dot (QD)-coated flat/hemiwicking surface

Fig. 1 showcases the experimental setup used in this investigation. Dip coating and drop-casting techniques are employed to trap quantum dots inside nanopores (d = 20-30 nm) of ceramic membranes and inexpensive paper. For this purpose, quantum dots-toluene solution of 20 mg/ml concentration is made. In this regard, non-toxic $CuInS_2$/ZnS quantum dots of size, d = 5nm and peak emission at 550 nm and 750 nm are chosen. This solution is undergone several ultrasonication baths to avoid settling of the nanoparticle inside the solution.

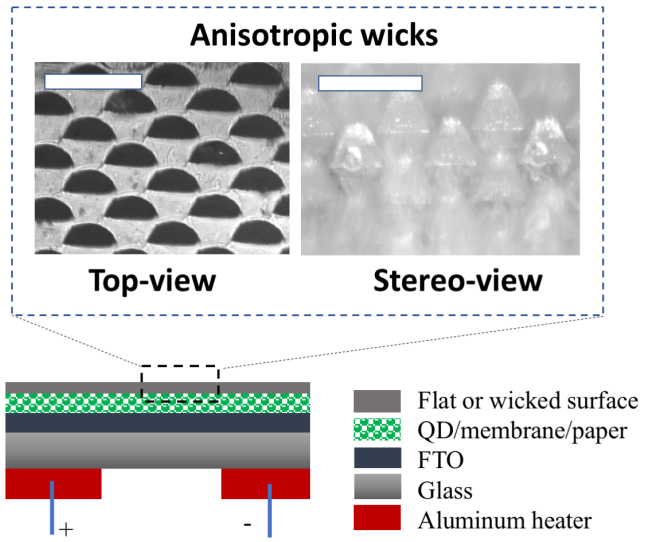

Fig. 2: Heater module: QD loaded nanomembrane/paper is attached onto Fluorine Tin Oxide (FTO) coated soda lime based glass substrate (thickness of 1.1 mm) using Norland Optical Adhesive (NOA). Here, the white line represents a length scale of 60μm.

Once the quantum dot nanoparticles are well suspended inside the toluene solvent, the suspension is transferred to the cuvette which acts as a dip-coating reservoir. A Teflon-made-holder holds the nanomembrane flake which is carefully aligned with the cuvette. During dip coating, three important features are tuned to achieve very uniform thin film of quantum dots. These features are the dipping velocity (5mm/s), waiting time (1s) and withdrawal velocity (0.05mm/s). During dip coating, due to capillary forces and surface wetting phenomenon, the quantum dots suspension wets the nanomembrane and thus nanoparticles tend to get trapped inside the nanopores. Once the withdrawal starts, the toluene solvent begins to evaporate off and all the quantum dots remain trapped after full withdrawal. Moreover, the drop-casting is

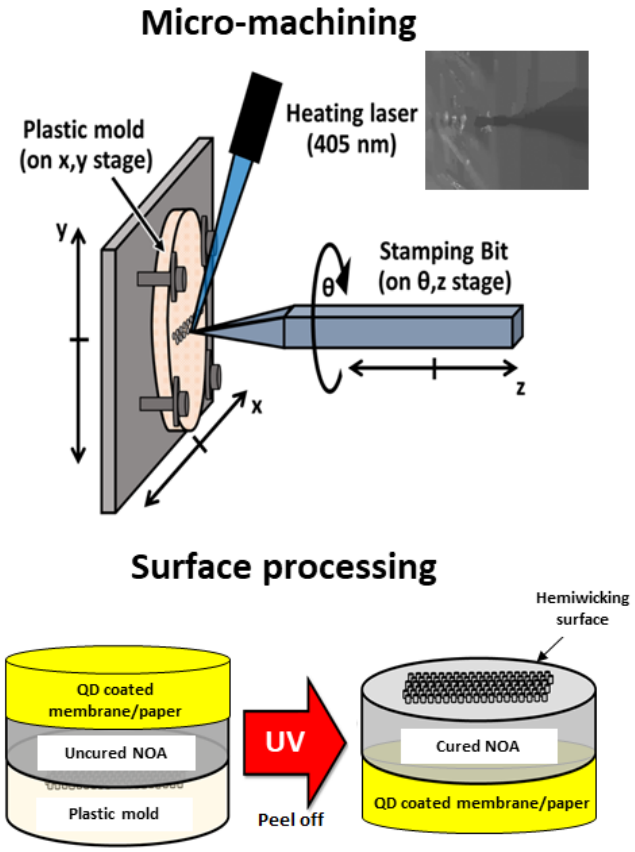

Fig. 3: Fabrication: hemiwicking surface using microstamped plastic mold [11]

performed at elevated temperature so that solvents get the chance to evaporate quickly without creating a “coffee-ring” effect on the paper. Once the uniform thin film of quantum dots is achieved, the saturated nanomembrane/paper is placed on ultrasonically cleaned Fluorine Tin Oxide (FTO) coated Boro-Silicate based glass substrate (see Fig. 2). To keep the nanomembrane/paper in place with the sample, the optically transparent epoxy (Norland Optical Adhesive 61) is used and cured inside a UV chamber. The sample is then attached with a resistive heater using highly conductive (k = 403 W/m-K) copper foils. Fig. 3 shows deetailed fabrication steps to

have hemiwicking surface. As shown in the illustration, a microscale drill bit pokes holes on a acrylic plastic window. A heating LASER (405nm of wavelength) heats locally and melts the drilling location before the poking happens. Thus, a pattern of microscale holes are found on the plastic sample. Later, NOA is poured into the plastic mold and Quantum Dot (QD) coated nanomembrane or paper is attached on the top. After 30 min of UV curing, the QD dot coated hemiwicking surface is found by peeling the layer off from the plastic mold.

As shown in Fig. 1, to excite the quantum dots with external means, high power diode laser (4W at 440nm) is used. A high speed laser scanner (galvanomirror), controlled by a LABVIEW program, scans the quantum dot coated region (1cm x 1cm) at frequencies, f_x, f_y = 133 Hz, 533 Hz and amplitude, A_x, A_y = 100 mm, 80 mm. The spectral information (e.g. photoluminescence) from the quantum-dot coated thin film is captured using an OceanOptics spectrometer at an integration time of 500 ms and sample rate of 6. It is to be noted that, a 500 nm filter is installed to filter out the contribution coming from the excitation laser.

CHARACTERIZATION

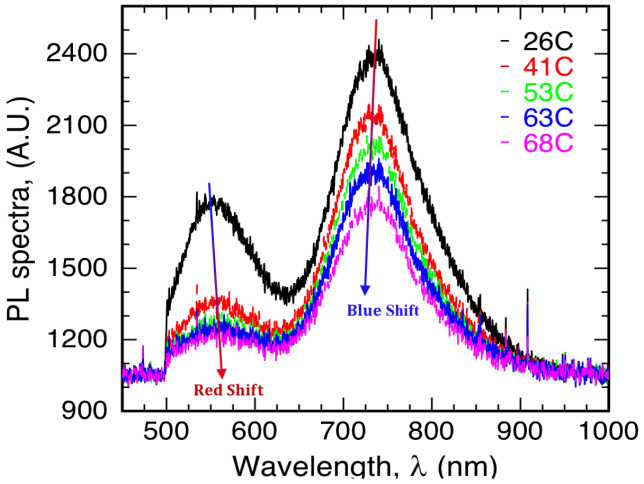

Fig. 4: Photoluminescence (PL) spectra profile as a function of wavelength for dual quantum dotted sample at P_{laser} = 3.5W for temperature levels from 26°C to 68°C

Fig. 4 illustrates the photoluminescence distribution over wavelength at excitation laser power of 3.5W. Intensity of the QDs at different temperature levels can be characterized by energy band configurations. A dual quantum dot coating (750nm and 550nm) is chosen as it serves better PL intensity range and significant blue/red-shifts. At high temperature level, the probability of radiation conversion decreases which leads to lower quantum yield. Additionally, as the temperature increases, exciton-optical phonon coupling and exciton-acoustic phonon coupling correspond to higher non-radiative recombination [12].

These recombinations are enhanced by atom's same-direction vibration (optical phonon) and opposite-direction-vibration (acoustic phonon) in the unit cell. Because of these

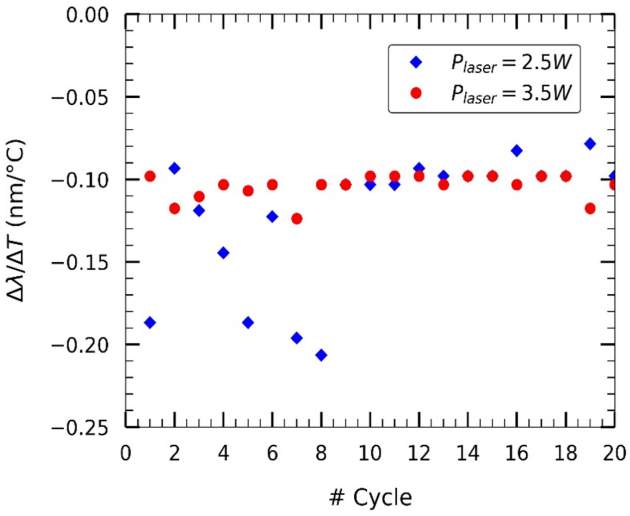

Fig. 5: The influence of heating-cooling cycle number on thermal fluorescence coefficient is provided in terms of wavelength shift gradient for excitation laser power of 2.5W and 3.5W. Thermal fluorescence coefficients ($\Delta\lambda/\Delta$T) is derived from spectra counts (A.U.) from spectrometer. For 20 different heating-cooling cycles spanning over 30 days, uniform thermal fluorescence coefficient of -0.1 nm/°C is observed. Spectral intensity gradient regains after relaxation time of 48hrs at 10th thermal cycle.

TABLE I: Influence of surface temperature on Photoluminescence (PL) peak intensity for dual quantum dot

$T_s(C)$	Intensity (750nm QD)	Intensity (550nm QD)
26	2350	1800
41	2100	1350
53	1940	1250
63	1800	1200
68	1650	1180

lower quantum yield and higher non-radiation recombination, the peak photoluminescence intensity of the 750nm QDs tends to decrease (from 2350 A.U. to 1650 A.U.) with a temperature increase from 26.0°C to 68°C (see Fig. 4). Moreover, it is evident from the same illustration that the peak emission intensity (for 750nm QDs) moves toward lower wavelength (blue-shift). This is mainly because of the interesting interplay between electron-phonon-renormalizations and thermal expansion. For all the semiconductors, the thermal expansion effect is assumed to be negligible and all the theoretical models are developed based on simplistic approach of electron-phonon interaction and that is how they show decreasing relationship of energy band with higher temperature (like Varshni's equation (Eq.1)) [13].

$$E_g = E_{g,o} - \frac{\alpha T^2}{T + \beta} \quad (1)$$

Here, α, β are the correlation constants. In contrast, in non-semiconductors, the thermal expansion has significant contri-

bution to the phonon density of states. These phonon-density of states can be determined from corresponding vibration frequency (for example in our case, 'Cu-like, In-like, S-like' vibrations. Dey et al. investigates some using PbS nanocrystals (and mentioned about 'Pb-like', 'S-like' vibrations). They come up with a model that combines effect of thermal expansion and electron-phonon-renormalization on energy band gap. Surprisingly they found increasing trend of energy band gap (blue-shift) with higher temperatures for non-semiconductor nanocrystals which justifies our reasoning as well. Such blue-shift is quantified for twenty different thermal quenching cycles. Thermal photoluminescence co-efficient ($\frac{\Delta\lambda}{\Delta T}$) is from the peak intensity shift (blue-shift) and plotted against quenching cycles in Fig. 5. It is evident from Fig. 5 that the system is highly stable since the photoluminescence coefficient remains uniform even at very high number of heating-cooling cycle. Thus these red/blue shifts play a significant role in determining this fluorescence technique's sustainability.

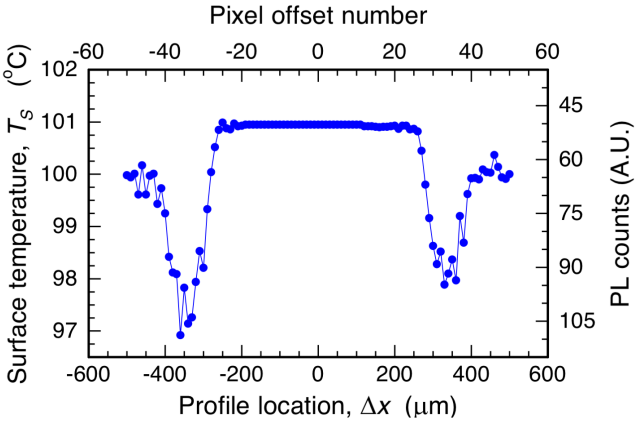

Fig. 7: Local Photo Luminescence (PL) intensity and temperature profile through the midline (rectangular ROI in Fig. 6) of the water droplet

APPLICATIONS

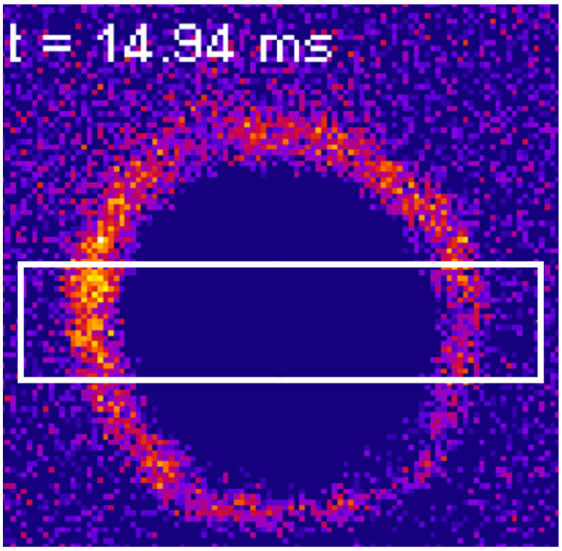

Fig. 6: Applications of the thermal mapping technique: Surface temperature measurements during droplet impingement cooling at t = 14.94ms

Once the photoluminescence characterization is completed, the Phantom high speed camera replaces the optical fiber and captures the scanned Region of Interest (ROI) at 3000 fps and 23 μs shutter time. Greyscale values (GSV) from visible imagery from the HSV is further analyzed for different temperature levels (23°C to 101°C). During the calibration phase, the GSV information is only captured for heating and nature convection air-cooling. The QD coated paper is attached with the FTO/glass substrate (FTO side) (see Fig. 2). The FTO glass is ohmically heated until the global surface temperature (measured by thermocouple) reaches the steady state at 100°C. First, the temperature calibration is performed against PL intensity values. From the data extracted at different temperature levels (see Table.1), a trend line is formed. Later, GSV values from the high speed camera is extracted for different surface temperature levels. Grey scale values are averaged over the number of pixels (inside the Region of Interest) for a corresponding temperature.

After the calibration is done, experiments were conducted on two different surfaces such as i) flat (for droplet impinging experiment), and ii) micropillared (for hemiwicking experiment) to test this mapping technique. Keeping the laser scanner and high speed camera 'ON', a micro droplet is dispensed on the QD coated paper (flat and micro pillared surfaces, separately). HSV captures the moments (from transient to steady) and data are post-processed to convert pixel-by-pixel GSV to pixel-by-pixel temperature values using calibration trend line (found from Fig. 4, and Table 1). As mentioned, to test this thermography technique, surface temperature during water droplet impingement cooling on a heated substrate (100°C) is captured and shown in Fig. 6 at t = 14.94ms. It is observed from the local temperature profile (in Fig. 7) through the midline of the droplet that there is a 3°C interface cooling at the edge of the droplet with a relatively hotter temperature (101°C) at the core of the droplet.

To further test the ability of this thermography technique to capture transient phenomena, thermal evolution during hemiwicking flows through anisotropic micro-pillared wicks is measured and shown in Fig. 8. Microstamping mechanism shown in Fig. 3 [11] is employed to create a plastic mold with micron scale holes. NOA is poured onto the holes and before starting the curing process inside UV chamber, QD-saturated paper is attached. Later, the NOA coated paper is peeled off from the mold carefully. Thus the anisotropic wicks are achieved which are shown as top-view in and stereo-view in Fig. 3. To facilitate the hemiwicking experiment, isopropanol droplet (25°C) is casted at the edge of the heated wicks (105°C). Due to gradient caused by the capillary force, the isopropanol film starts to propagate. Figure shows that hemiwicking front generates enormous cooling effect (105°C

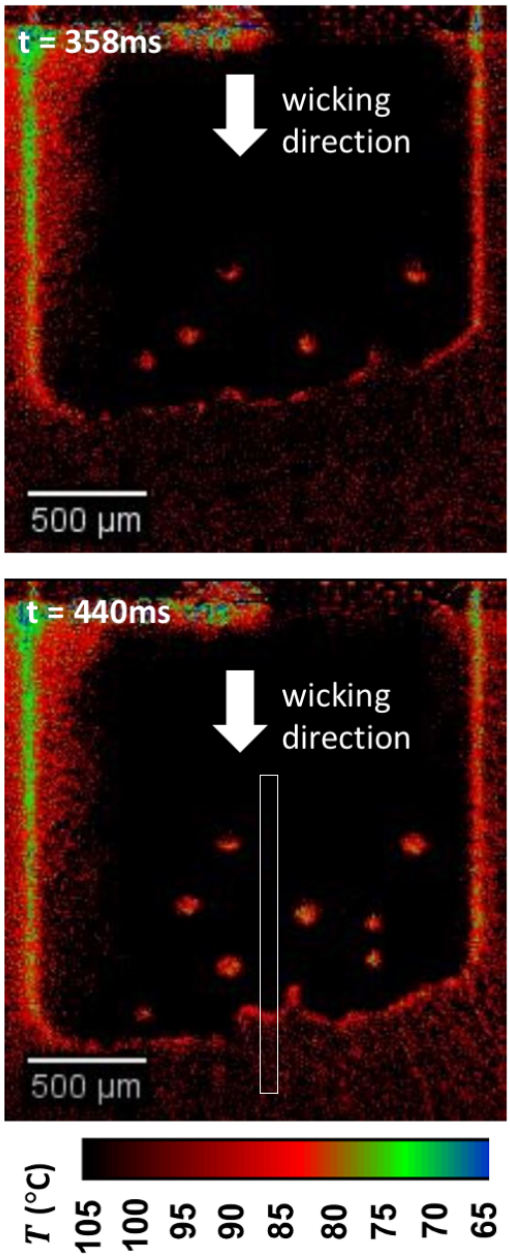

Fig. 8: Applications of low-cost thermal mapping technique: temperature evaloution of the hemiwicking front at t= 358 ms and 440 ms

to 70°C) during such propagation on the heated substrate (105°C) at t = 358 ms and 440 ms. It is to be noted the non-uniforimty in thermal maps in left portions of both droplet impingement and hemiwicking are because of the non-uniform distribution of intensity.

This transient temperature changes very interestingly as it wicks the surface. Fig. 9 shows local surface temperature profile and PL counts at midline of the hemiwicking surface (along the wicking direction). This pixel-by-pixel thermal information can be used to get wicking front speed by implementing the thermal and momentum diffusion at the

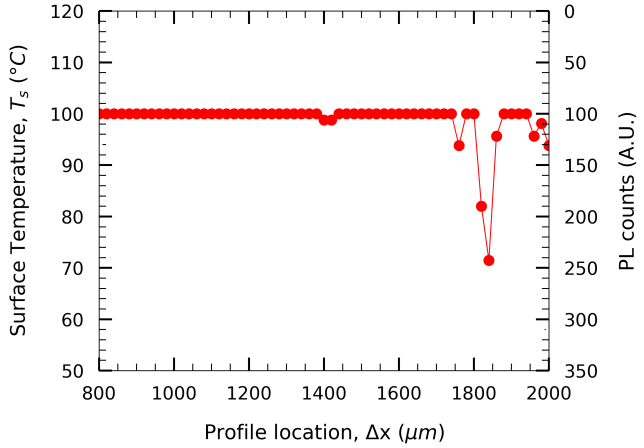

Fig. 9: Local Photo Luminescence (PL) intensity and temperature profile through the midline (rectangular ROI in Fig. 8) of the hemiwicking surface

solid-liquid interface. On dynamics of hemiwicking, Kim [14] provided a scaling relation stated below-

$$L\alpha\sqrt{\frac{\gamma\eta ht}{\mu}} \tag{2}$$

Here, L, γ, η, h, t, μ are wicking front distance, surface tension, generalized coefficient, wicking micro-pillar height, and time-elapsed, respectively. Whereas, Choi et al. [15] provided insights about fluid refreshing through these hemiwicking surface can augment Critical Heat Flux (CHF) by 100%. Therefore, the transient thermal information of hemiwicking surface, given by this novel thermal mapping technique, will provide important design guidelines (geometry and fluid properties) to fabricate future generation thermal management technologies such that it can handle high heat fluxes.

CONCLUSION

This paper introduces a novel technique to design and fabricate a thermal sensor using $CuInS_2$/ZnS quantum dots (5-10nm, in diameters) loaded ceramic nanoporous membrane or everyday use paper. A low-cost and effective dip-coating and/or drop casting technique is employed to achieve uniform thin film of quantum dots. Spectral information is captured while a excitation laser scans the quantum dotted interface at frequencies of 133 Hz (axial) and 533 Hz (longitudinal). Thermal characterization experiments reveal the sensor's capability to capture thermal information with a sustained thermo-photoluminescence coefficent of -0.1nm/°C. Moreover, the thermal quenching trials ensure higher order stability of such interface even at higher number of thermal cycles with intermittent thermal relaxation events. Finally, this thermal mapping technique is employed to perform thermal mesurements during droplet impingement cooling and hemiwicking flows on anisotropic micropillared surface. With such spatio-temporal benefits, this low-cost mapping technique can be used to capture useful thermal

information during transient cooling in micron-to-nanoscale sized electronic devices, especially at high thermal loads. Thus, it will provide important design guidelines for future generation cooling systems for uninterrupted operations of devices.

Acknowledgments

This material is based on research partially sponsored by the U.S. Office of Naval Research under Grant No. N00014-15-1-2481 and the National Science Foundation under Grant No. 1653396. The views and conclusions contained herein are those of the authors and should not be interpreted as necessarily representing the official policies or endorsements, either expressed or implied, of U.S. Office of Naval Research, the National Science Foundation, or the U.S. Government.

References

[1] A. Richenderfer, A. Kossolapov, J. H. Seong, G. Saccone, E. Demarly, R. Kommajosyula, E. Baglietto, J. Buongiorno, and M. Bucci, "Investigation of subcooled flow boiling and chf using high-resolution diagnostics," *Experimental Thermal and Fluid Science*, vol. 99, pp. 35–58, 2018.

[2] M. Mehrvand and S. A. Putnam, "Transient and local two-phase heat transport at macro-scales to nano-scales," *Communications Physics*, vol. 1, no. 1, p. 21, 2018.

[3] E. Peinke, T. Sattler, G. M. Torelly, J. Bleuse, J. Claudon, W. L. Vos, and J.-M. Gérard, "Generation of ultra-short (˜ 10ps) spontaneous emission pulses by quantum dots in a switched optical microcavity," *arXiv preprint arXiv:1910.10518*, 2019.

[4] L. M. Maestro, C. Jacinto, U. R. Silva, F. Vetrone, J. A. Capobianco, D. Jaque, and J. G. Solé, "Cdte quantum dots as nanothermometers: towards highly sensitive thermal imaging," *Small*, vol. 7, no. 13, pp. 1774–1778, 2011.

[5] L. M. Maestro, E. M. Rodriguez, F. S. Rodriguez, M. I.-d. la Cruz, A. Juarranz, R. Naccache, F. Vetrone, D. Jaque, J. A. Capobianco, and J. G. Sole, "Cdse quantum dots for two-photon fluorescence thermal imaging," *Nano letters*, vol. 10, no. 12, pp. 5109–5115, 2010.

[6] S. Li, K. Zhang, J.-M. Yang, L. Lin, and H. Yang, "Single quantum dots as local temperature markers," *Nano letters*, vol. 7, no. 10, pp. 3102–3105, 2007.

[7] P. Haro-González, L. Martínez-Maestro, I. Martín, J. García-Solé, and D. Jaque, "High-sensitivity fluorescence lifetime thermal sensing based on cdte quantum dots," *Small*, vol. 8, no. 17, pp. 2652–2658, 2012.

[8] S. Keuleyan, E. Lhuillier, V. Brajuskovic, and P. Guyot-Sionnest, "Mid-infrared hgte colloidal quantum dot photodetectors," *Nature Photonics*, vol. 5, no. 8, p. 489, 2011.

[9] C. Chapman, Y. Liu, G. Sonek, and B. Tromberg, "The use of exogenous fluorescent probes for temperature measurements in single living cells," *Photochemistry and photobiology*, vol. 62, no. 3, pp. 416–425, 1995.

[10] D. J. Norris, "Multispectral quantum-dot photodetectors," *Nature Photonics*, vol. 13, no. 4, p. 230, 2019.

[11] T. Germain, C. Brewer, J. Scott, and S. A. Putnam, "Scalable stamp printing and fabrication of hemiwicking surfaces," *JoVE (Journal of Visualized Experiments)*, no. 142, p. e58546, 2018.

[12] J. Yang, Z. Ling, B. Q. Li, R. Li, and X. Mei, "Nanoscale 3d temperature gradient measurement based on fluorescence spectral characteristics of the cdte quantum dot probe," *Optics express*, vol. 27, no. 5, pp. 6770–6791, 2019.

[13] Y. P. Varshni, "Temperature dependence of the energy gap in semiconductors," *physica*, vol. 34, no. 1, pp. 149–154, 1967.

[14] J. Kim, M.-W. Moon, and H.-Y. Kim, "Dynamics of hemiwicking," *Journal of Fluid Mechanics*, vol. 800, pp. 57–71, 2016.

[15] B. S. Kim, G. Choi, D. I. Shim, K. M. Kim, and H. H. Cho, "Surface roughening for hemi-wicking and its impact on convective boiling heat transfer," *International Journal of Heat and Mass Transfer*, vol. 102, pp. 1100–1107, 2016.